Review Article

http://dx.doi.org/10.4322/2176-1523.1092

APPLICATION OF THE CALPHAD METHOD FOR FERRITIC BOILER STEELS

André Schneider[I]

Abstract

Some applications of the CALPHAD method are shown with reference to seamless tubes and pipes for high-temperature service in power plants. The focus is on concepts on the improvement of creep strength. In view of developing or improving steels for the application in conventional power plants, various elements have been tested with respect to a controlled precipitation of chromium carbides, carbonitrides and the intermetallic Laves phase.The kinetic simulations are focussed on diffusion-controlled transformations during heat-treatment and application in the power plant. A key-issue is to include important aspects such as nucleation density (in terms of pre-defined cell sizes of the model), growth, and dissolution of precipitates.
Keywords: Steel; CALPHAD; Boiler; Diffusion simulation; Microstructure.

APLICAÇÃO DO MÉTODO CALPHAD A AÇOS FERRÍTICOS PARA CALDEIRAS

Resumo

Algumas aplicações do método CALPHAD a tubulações para aplicação a alta temperatura em plantas termoelétricas de alta temperatura são apresentadas. O trabalho é focalizado no desenvolvimento de concepções que resultem em aumento da resistência a fluência. Visando desenvolver e aprimorar aços para a aplicação em usinas térmicas convencionais vários elementos de liga foram investigados com vistas a precipitação controlada de carbonetos de cromo, carbonitretos e a fase intermetálica de Laves. As simulações cinéticas são focadas em transformações controladas por difusão que ocorrem durante o tratamento térmico e durante a aplicação do aço nas usinas. Um ponto chave é a inclusão de aspectos importantes como a densidade de núcleos (expressa como um tamanho de célula pré-definido no modelo), o crescimento e a dissolução dos precipitados.
Palavras-chave: Aço; CALPHAD; Caldeiras; Simulação de difusão; Microestrutura.

1 INTRODUCTION

Main parts of conventional power plants are built of a variety of seamless tubes and pipes. Figure 1 illustrates the application of ferritic and austenitic steels in the currently existing ultra super-critical (USC) technology and their respective potential usage in the future advanced ultra super-critical (A-USC) technology, which is considered also to incorporate Nickel-based alloys. The efficiency is intended to be increased from 45% for USC up to 50% for A-USC by increasing the steam parameters from up to 300 bars and 600°C towards 700°C and 350 bars. Figure 1. Boiler Materials used for the current USC and the future A-USC technology [1].

Figure 2 shows an example of the production of large diameter and thick wall tubular products at Vallourec Reisholz mill according to the Ehrhardt process (see [1]). Vallourec is a world leader in its markets and provides tubular solutions that are the benchmark reference for the energy sector and other applications that present the most demanding challenges. The Group relies on its six Research and Development centers worldwide and more than 500 researchers to maintain its technological leadership and meet its customers' latest requirements. Figure 2 illustrates that tubes and pipes for power plant applications undergo various temperature cycles during production before being continuously exposed to high temperatures during service operation. The production processes result in microstructural changes of the steels. Typical heat-treatments of 9-12%Cr steels is normalization (1020 – 1070°C) and heat-treatment at 730 – 780°C [2-3].

[I] *Vallourec Research Center Germany, Düsseldorf, Germany. E-mail: andre.schneider@vallourec.com*

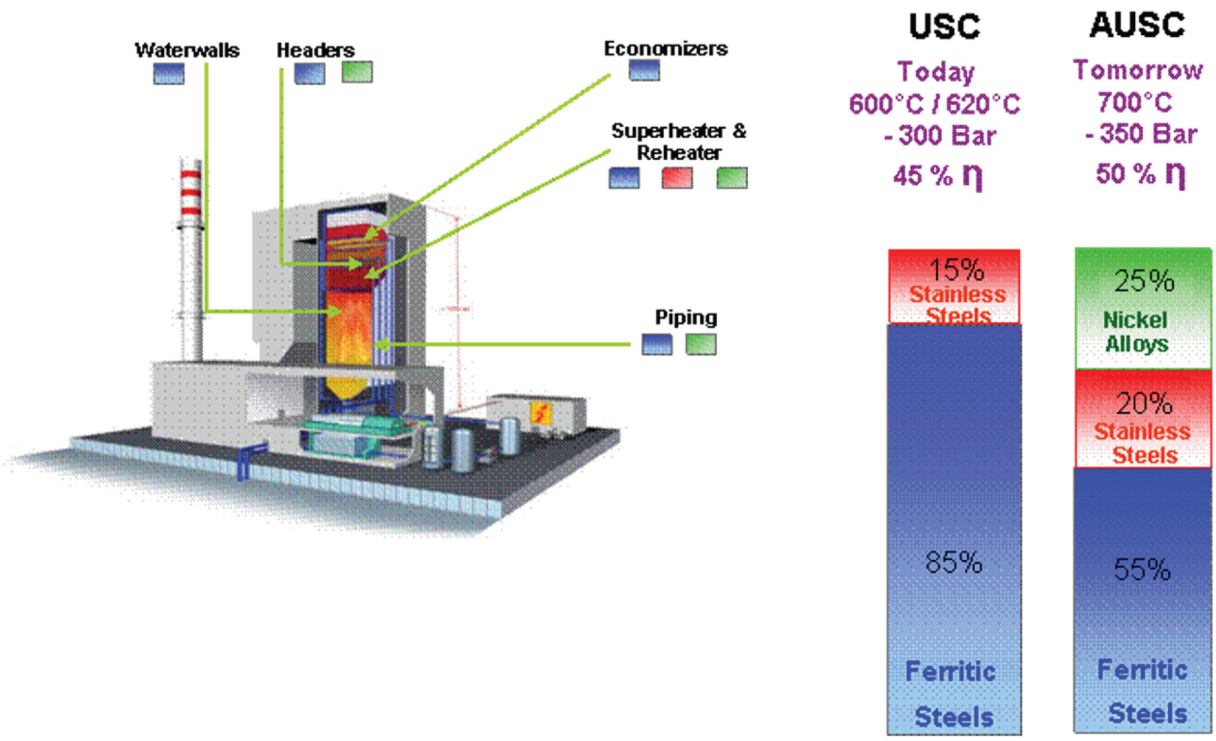

Figure 1. Boiler Materials used for the current USC and the future A-USC technology [1].

Figure 2. Manufacturing of tubular goods in the Vallourec Reisholz mill according to the Ehrhardt process: (a) piercing, (b) drawing, (c) final product [1].

In order to meet the requirements with respect to increasing steam parameters the performance of materials used in power plants need to be improved [1]. This paper refers to some examples of how the so-called CALPHAD approach [4-7] can be applied in the frame of boiler materials development.

2 EQUILIBRIUM

In the framework of alloy design, chemical elements are usually classified according to their stabilizing effect on various phases such as ferrite or austenite. The stabilizing effect of an element is determined by its effect on the phase boundaries. Thus, an element leading to a widening of the ferrite phase field is called ferrite stabilizer. The same holds for austenite stabilizing elements. This effect is quantitatively scaled relative to the reference elements Cr (ferrite stabilizers) and Ni (austenite stabilizers). Using this approach a so-called Schaeffler diagram modified according to H. Schneider [8] can be constructed [3] by introducing so-called Cr- and Ni-equivalents. An early version of such a Schaeffler diagram has been used for welding [9]. Such a diagram is very useful for determining the limits for the occurrence of δ-ferrite after austenitization treatment (normalization). The various candidate alloy compositions

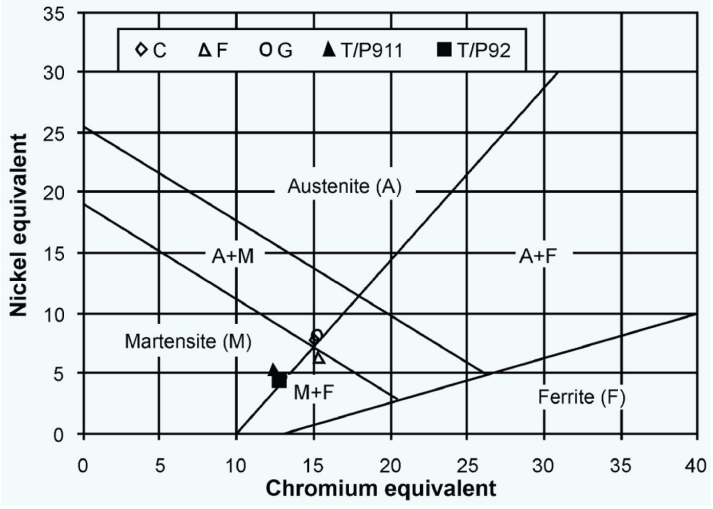

Figure 3. Schaeffler diagram modified according to H. Schneider [8] (Cr-eq= Cr+2Si+1.5Mo+5V+5.5Al+1.75Nb+1.5Ti+0.75W/ Ni-eq=Ni+Co+0.5Mn+30C+0.3Cu+25N) [3].

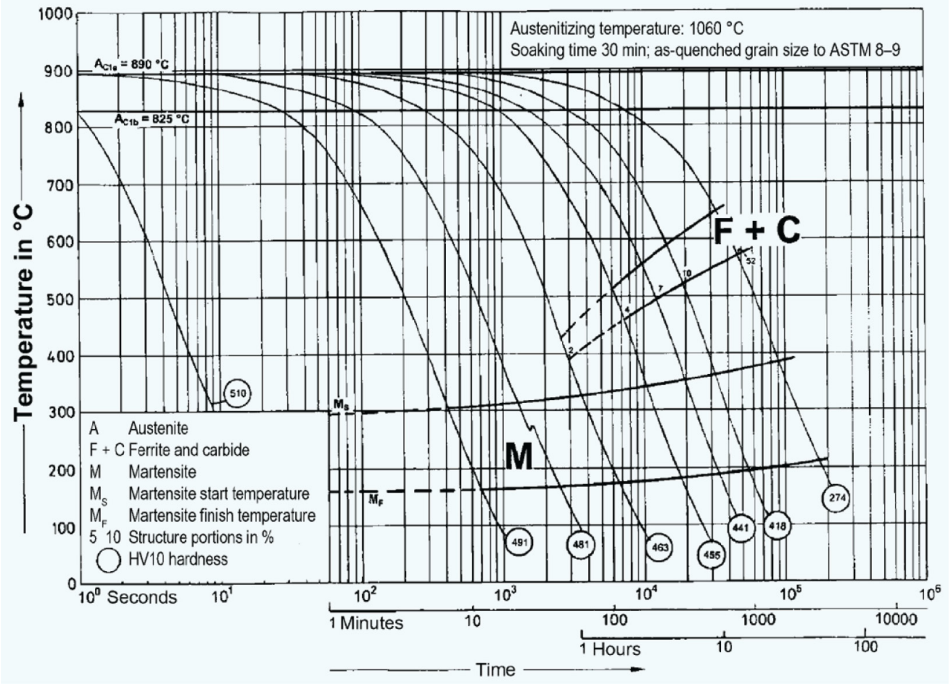

Figure 4. CCT diagram for the steel VM12-SHC [3].

can be introduced in this diagram (see Figure 3) in order to predict (with a certain probability) the nature of the resulting microstructure.

An optimal result for a martensitic/ferritic 9-12Cr steel is to be positioned in the lower left area (100% martensite). For example, the boiler tube grade VM12-SHC shows a CCT diagram allowing for reaching a martensitic microstructure after cooling (Figure 4).

The applicability of such Schaeffler diagrams is proven to be reliable by checking the limits of extrapolation of the various stabilizing elements [10]. Such calculated data show quantitatively for each alloying element in what extent they can be reliably calculated following the equations represented in Figure 3. The calculated isothermal sections for the ternary system Fe-Ni-Cr at 800, 1000, and 1200°C in Figure 5 clearly show that the choice of the austenitization temperature determines the positioning of the phase boundaries between the γ- and α-fields. Thus, it is an important boundary condition for the application of the Schaeffler diagram. The tie-lines in Figure 5 determine the equilibrium chemical composition of the phases in the two-phase equilibria.

The ferrite stabilizer Vanadium is chosen for the calculation (using Thermo-Calc) of the effect of V on the

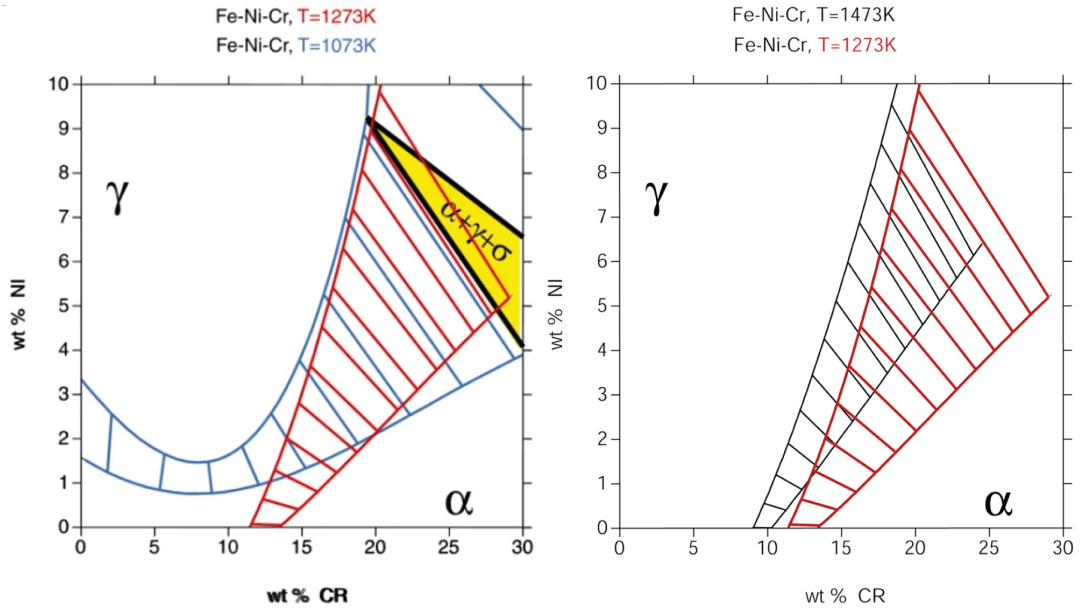

Figure 5. Calculated isothermal sections for the ternary system Fe-Ni-Cr at 800, 1000, and 1200°C.

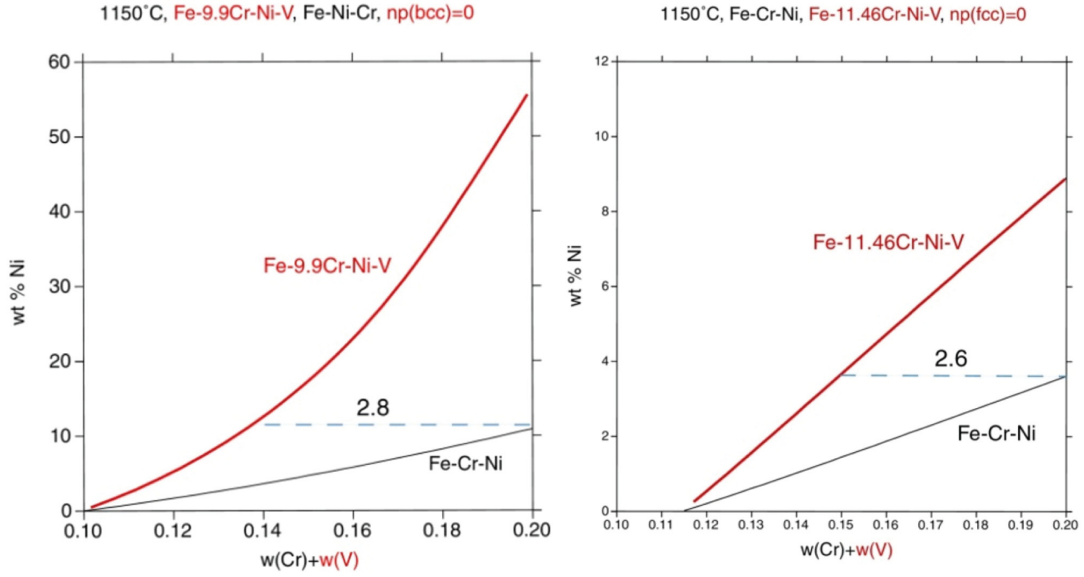

Figure 6. Calculated effect of V on the solubility limits of ferrite and austenite relative to the effect of Cr at 1150°C. The factors 2.8 and 2.5 are the Cr-equivalent factors of V (according to [10]).

solubility limits of ferrite and austenite relative to the effect of Cr at 1150°C (see Figures 6 a, b). It can be clearly seen that V leads to a widening of the ferrite phase field. The Cr-equivalent factors vary between 2.5 and 2.8. Such calculated results are used in addition to the experimentally determined ones available in literature by searching for the best compromise, since also the experimental data can be very different.

Another way of using thermodynamic calculations is illustrated in Figure 7 showing the amount of δ−ferrite (left) at 1070°C and A_1 temperature (right) as a function of the amount of the respective alloying element (austenite stabilizers Cu, Ni, Co, and Mn). The possibility to calculate different types of diagrams for binary, ternary, and higher order systems is one of the strengths of the thermodynamic calculations.

In the following, it is shown how computational thermodynamics can be used to reduce the number of laboratory heats in the framework of an alloy design including testing the mechanical, especially creep properties [11]. The example is taken from a study on novel heat-resisting martensitic/ferritic steels for application in conventional power plants with service temperature of 650°C. The creep resistance should be achieved by a well-balanced choice of alloying elements for controlled precipitations of $M_{23}C_6$ carbides, MX carbo-nitrides, and the intermetallic Laves phase. With respect to the above mentioned heat-treatment temperatures and the application temperature the boundary conditions are give as follows. In order to introduce a significant amount of Laves phase at application temperature one has look at the diagrams shown in Figure 8. It can be deduced from these diagrams how much of the Laves phase forming elements Mo, W, Nb, and Ta is needed to result in the respective precipitation reaction and appropriate volume fraction. The other pre-condition is set by the austenitization temperature. The two parameters T and x(Mo,W,Nb,or Ta) need to be within the γ-field in order to result in a fully martenistic microstructure (see also the above mentioned explanation, Figures 3 and 4). A similar consideration is included for the heat-treatment. Here the equilibrium diagram should show a significant tendency for the formation of $M_{23}C_6$. Although all four elements are indeed Laves phase forming elements, only the alloy systems containing Mo and W fulfill the requirements within a certain, limited composition range ($1.2 < \%Mo < 2$, and $1.2 < \%W < 3.7$). Niobium and Tantalum lead to shrinkage of the γ-field and therefore their amount cannot be increased above 0.3 wt% with respect to keeping a single γ-phase field. On the other hand their contents must be above 1 wt.% Nb and 1.9 wt.% Ta in order to achieve Laves phase at service temperature. Thus, these variants can be excluded from further considerations, i.e. no lab heat is to be cast for these compositions.

Certainly, the validity of the models needs to be proven experimentally for various cases, as it is demonstrated in Figure 9. The light-optical microscopy (LOM) and also the transmission electron microscopy (TEM) results reveal a microstructure in accordance with the tendency deduced from the equilibrium diagram (calculated mole fractions of phases as a function of temperature for Fe-11.85Cr-0.39Si-0.135C-0.055N-4.02W-0.19V-4.45Co-0.28Mn-1.0Cu-0.0068B). Such complex systems are not likely to reach equilibrium within reasonable time periods, but the equilibrium results are useful to identify the "direction towards equilibrium" predicting (with a certain probability) the phases being formed.

3 KINETICS

In this section the application of the software DICTRA is shown for some model assumptions which should show the general directions and kinetics of phase transformations. DICTRA is the abbreviation for DIffusion Controlled phase TRAnsformations and was developed by J. Ågren and G.

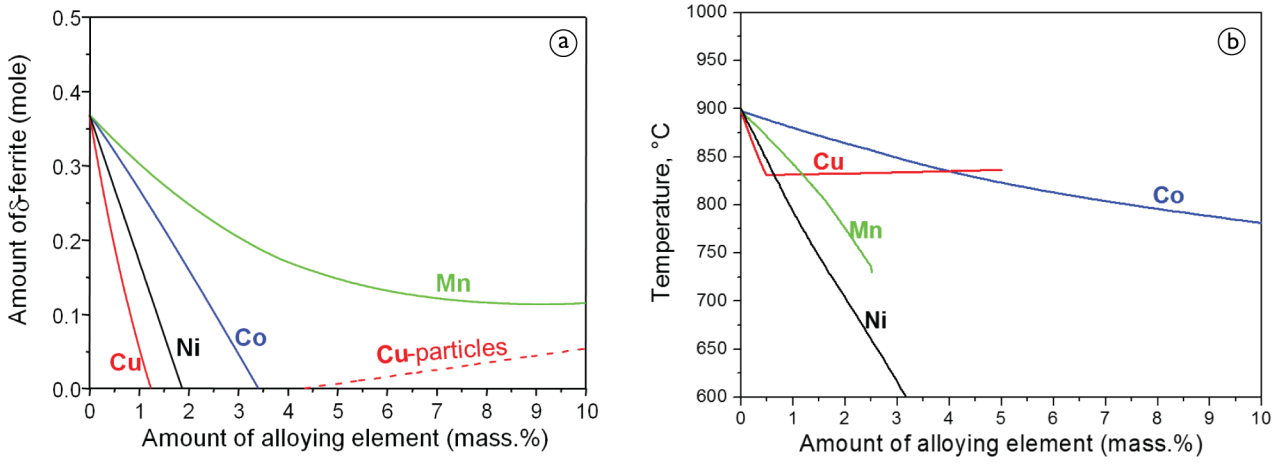

Figure 7. (a) The effect of austenite stabilisers on the amount of δ-ferrite at 1070°C, and (b) the effect of austenite stabilisers on the A_1 temperature of a 12Cr-0.15C-0.05N-0.2Si-0.2V-4W steel (wt.%) calculated by Thermo-Calc [11].

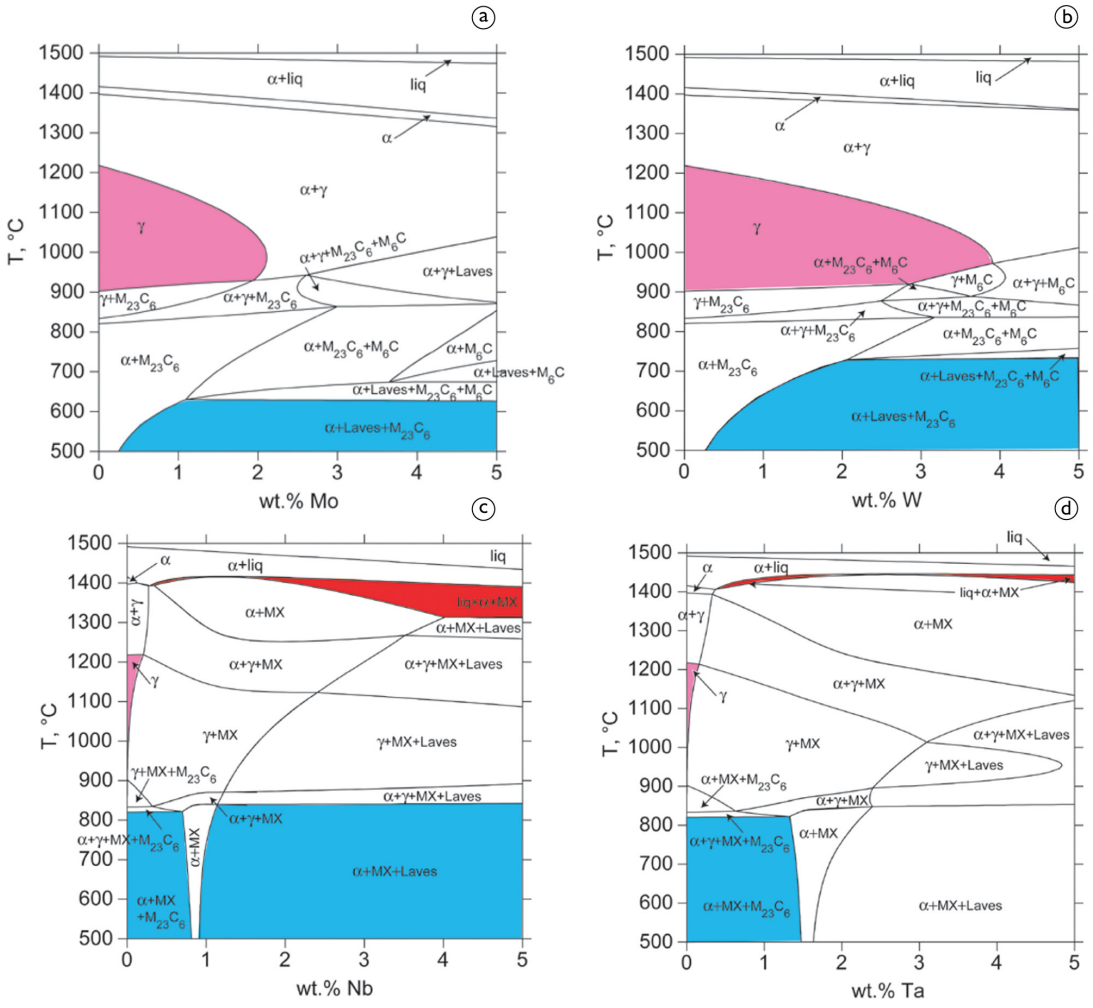

Figure 8. Phase diagram sections of the system Fe-12Cr-4.95Co-0.2Si-0.2V-0.1C (wt.%) with addition of (a) Mo, (b) W, (c) Nb, and (d) Ta, calculated using Thermo-Calc [11].

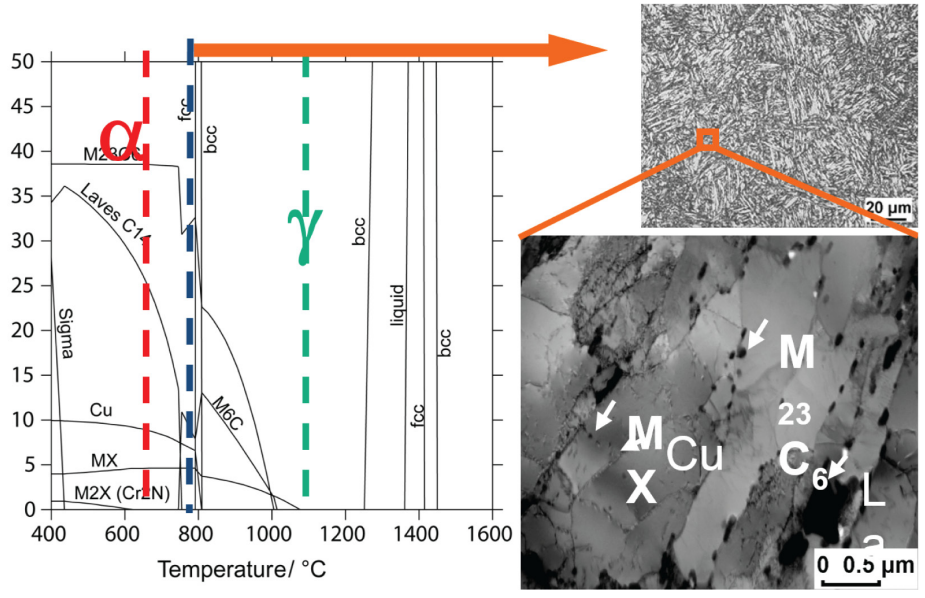

Figure 9. Calculated mole fractions of phases as a function of temperature for Fe-11.85Cr-0.39Si-0.135C-0.055N-4.02W-0.19V-4.45Co-0.28Mn-1.0Cu-0.0068B and related microstructures by LOM (upper micrograph) and TEM (lower micrograph), according to [11-12].

Inden et al. [13-17]. The fundamental concepts and model assumptions for this work are described in [18-19].

For a better understanding of the simulation results, only simple systems (Fe-Cr-C, Fe-Cr-Si-C, Fe-Cr-W-Mo-C, etc.) are chosen for the study on the effect of growth and dissolution of metastable phases on the growth of stable phases. In a first step, equilibrium calculations are performed to get an idea of how to define the set-up of the kinetic simulation. The corresponding diagrams in Figure 10 show equilibria for various Cr contents (left diagram). It can be seen that the alloy with 12Cr shows a stable equilibrium $\alpha+M_{23}C_6$ whereas the one with 7.3Cr shows $\alpha+M_7C_3$. For the consideration of an alloy composition (e.g. Fe-12Cr-0.1C) which will show carbide precipitation within a 100% ferritic matrix it makes sense to consider the so-called iso-activity lines. These lines will give a hint of driving forces towards

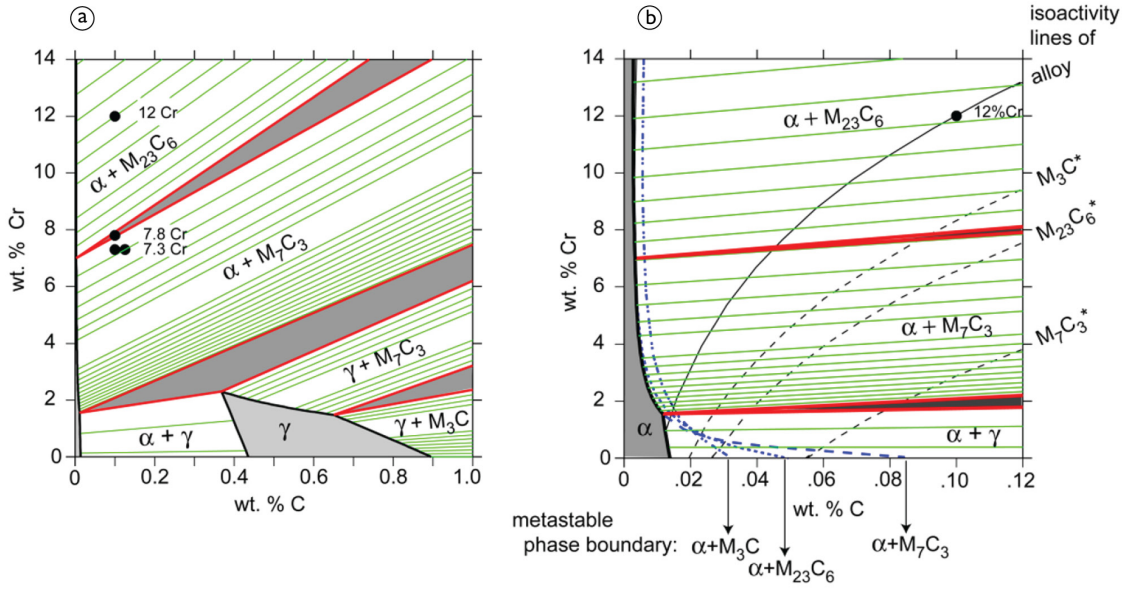

Figure 10. (a) Calculated isothermal section of the Fe-Cr-C phase diagram at 800°C. The various points represent model alloys used for the simulations reported in [18]. (b) Blowing-up of the diagram in a) showing the metastable extensions of the various phase boundaries. The point defines the alloy Fe-12Cr-0.1C. The various lines represent iso-activity curves in ferrite corresponding to the carbon activity of the carbides (M_3C, M_7C_3, $M_{23}C_6$) with the same Cr/Fe ratio in the alloy. This consideration is useful with respect to the discussion of the phase transformation kinetics (see [18]).

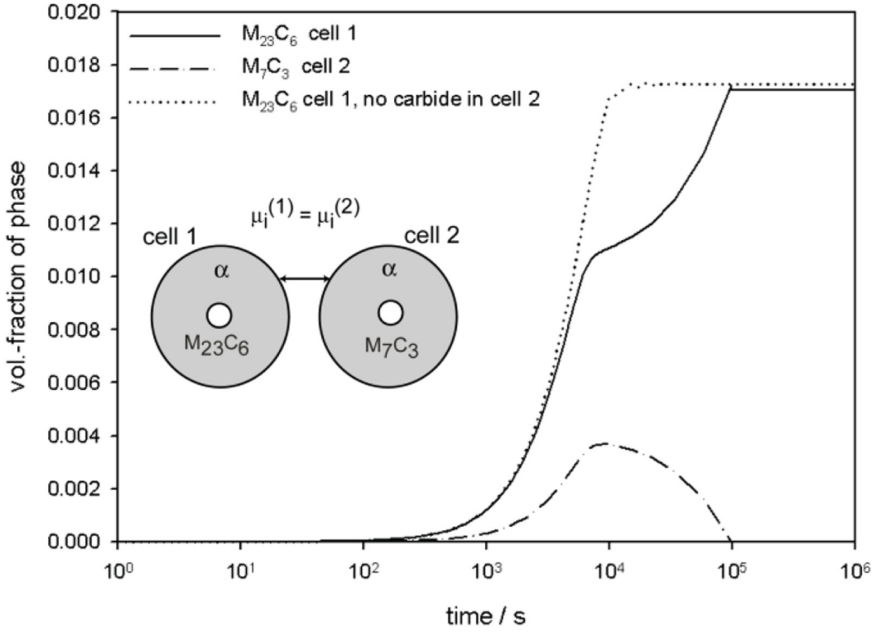

Figure 11. Two-cell simulation of competitive growth of stable $M_{23}C_6$ and metastable M_7C_3 in Fe-12Cr-0.1C at 800°C [18].

growth of stable and also metastable carbides. It should be mentioned that the definition of the matrix to be best represented by ferrite is a simplified condition which differs from the real case, i.e. martensite. Carbide nuclei have to be defined as a starting condition for the DICTRA simulation.

In Figure 11 two simulations are shown. One is on growth of stable $M_{23}C_6$ only which is reaching saturation at around 20000s. The second simulation is on simultaneous growth of stable $M_{23}C_6$ and metastable M_7C_3 (starting to shrink at around 10000s). The time period until the equilibrium volume fraction of $M_{23}C_6$ is reached is significantly prolonged.

The composition profiles in Figure 12 show another interesting effect. The local equilibrium at the moving phase interfaces α/M_7C_3 and also $\alpha/M_{23}C_6$ changes continuously during the reaction. This leads to the assumption that the carbides show a composition profile ones they are formed.

The importance of combining thermodynamics and kinetics becomes evident by looking at the following example. In Figure 13 the volume fraction of $M_{23}C_6$ is plotted versus time for different steels, one ternary Fe-Cr-C, and two additional ones with Si or Co. The elements Si and Co are considered not to be dissolved in $M_{23}C_6$, therefore the carbide can only grow by pushing Si or Co ahead of the moving phase interface. With respect to kinetics, this should result in a retardation of the reaction. This is indeed the case for the alloy with Co, but not for the alloy with Si (Figure 13). This can be understood by considering the effect of Si on the activity in ferrite. Silicon increases both

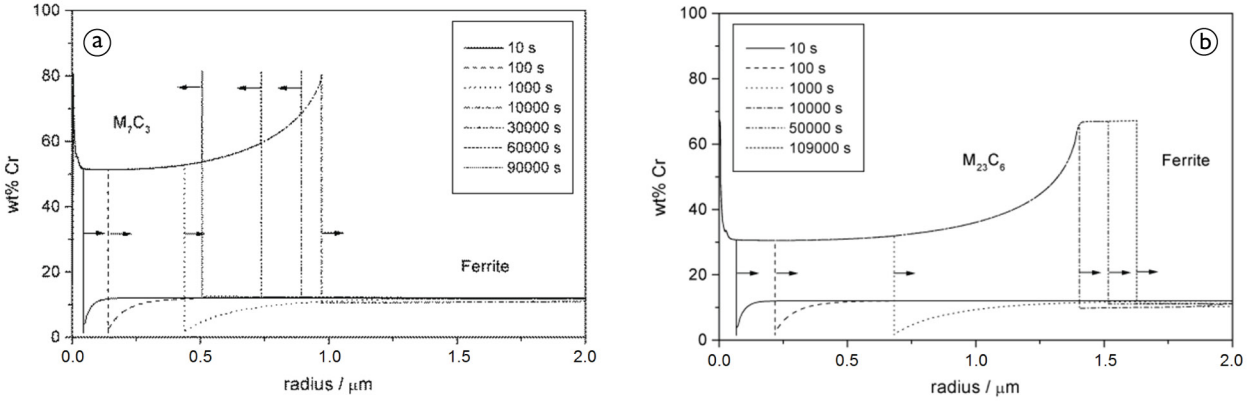

Figure 12. Composition profiles of Cr in (a) M_7C_3 and (b) $M_{23}C_6$ at various time steps (1nm nucleus, two coupled spherical cells with r=5μm) [18].

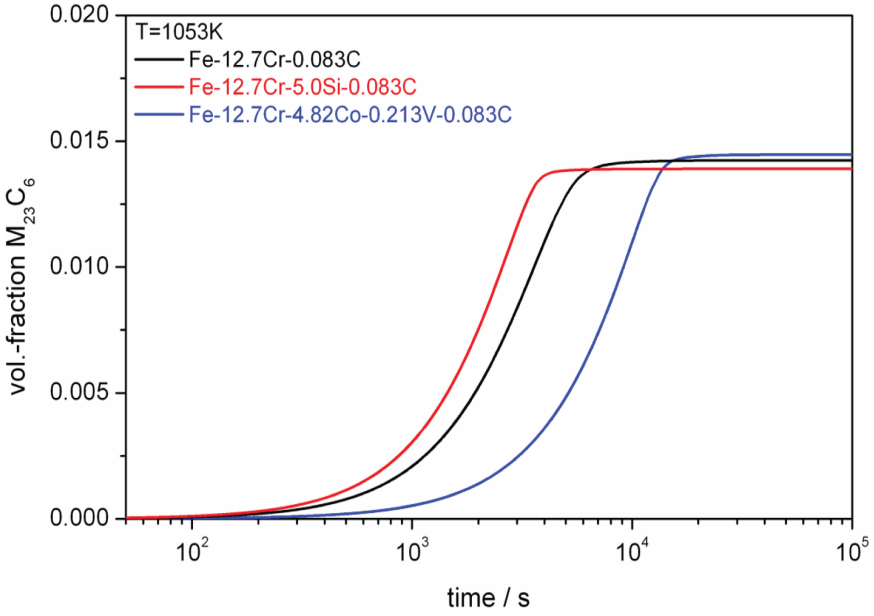

Figure 13. Fraction of $M_{23}C_6$ phase formed during precipitation reaction at 780°C in various ferritic steels. The simulations were performed for spherical cells of 5 μm in radius. The starting particle was 1 nm (according to [18]).

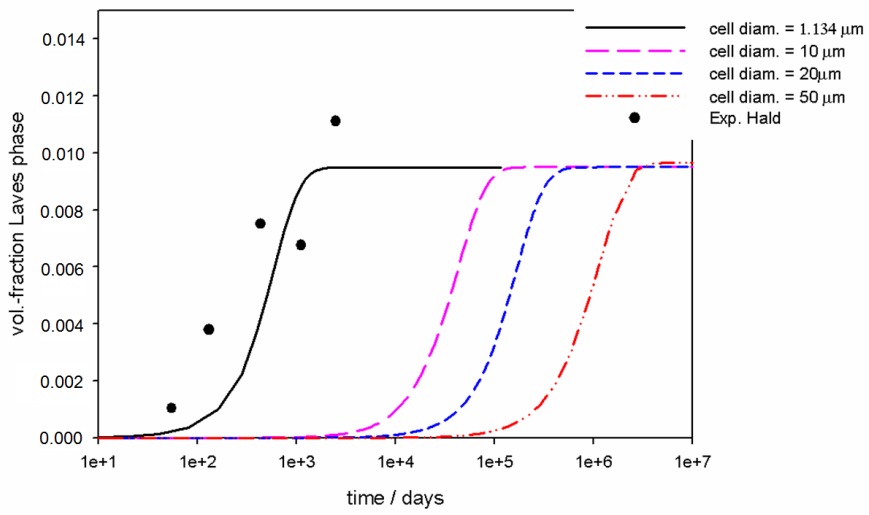

Figure 14. Volume fraction of Laves phase formed in Fe-8Cr-0.34Mo-1.65W-0.173C at 600°C. The calculation was performed for different cell sizes. Experimental data are added from [20]. The average particle distance in these experiments was determined as 1.1μm [18].

the C- and Cr-activity. This leads to a higher driving force for the reaction and to an increased growth velocity.

In ferritic steels with W as an alloying element, the Laves phase can come into play. Again, a simplified approach is chosen to understand how the simulation can represent the processes observed in reality (in experiments). The kinetic behavior of precipitation strongly depends on the cell size defined in the DICTRA simulation. In the cases shown above, the cell size was arbitrarily chosen and kept constant in order to make the results comparable to each other. In the following study the simulation on Laves phase growth in a Fe-8Cr-0.34Mo-1.65W-0.173C alloy at 600°C was performed choosing various cell sizes. By comparing the results with experimental findings from J. Hald et al. [20], the best fitting cell size is determined to be 1.13 μm (see Figure 14).

There are many further examples of applying CALPHAD for ferritic boiler steels [21-23]. The growth, dissolution, and coarsening of precipitates during long-term service at high temperatures is also tackled by various authors using DICTRA [24-28]. In addition to the concepts discussed in this paper there is also an approach developed by E. Kozeschnik including more elements in the simulations and with the possibility to define complex temperature profiles. Examples on long-term predictions by Mat-Calc concerning microstructural evolution in boiler steels - also including dissimilar welds - are given by [29-31].

4 SUMMARY

CALPHAD thermodynamics is a strong and useful tool in the frame of alloy development. It is applied by academia and also by industry to tackle various questions concerning alloy design or kinetics of phase transformations. This work refers to some examples on application of Thermo-Calc and DICTRA for martensitic/ferritic Cr steels.

REFERENCES

1 Dieulin A, Landier C, Subanovic M, Knezevic V, Cini E, Schneider A. V&M's innovative contribution to meet the challenges of present and future conventional power plants. VGB PowerTech. 2011;11:63-68.

2 Hahn B, Bendick W. Pipe steels for modern high-output power plants. Part 1: metallurgical principles – long-term properties: recommendations for use. 3R intern. 2008;47:3-12.

3 Hahn B, Bendick W. Pipe steels for modern high-output power plants. Part 1: metallurgical principles – long-term properties: recommendations for use. Düsseldorf: Vallourec Publication; 2015 [cited 2016 Feb 4] Available from: http://www.vallourec.com/fossilpower/EN/E-Library.

4 Kaufman L, Bernstein H. Computer calculation of phase diagrams. New York: Academic Press; 1970.

5 Saunders N, Miodownik AP. CALPHAD. In: Cahn RW, editor. Pergamon Materials Series. Oxford: Elsevier Science; 1998. vol. 1.

6 Lukas H, Fries SG, Sundman B. Computational thermodynamics: the CALPHAD method. Cambridge: Cambridge University Press; 2007.

7 Hack K, editor. The SGTE casebook: thermodynamics at work. London: The Institute of Materials; 1996.

8 Schneider H. Investment casting of high-hot strength 12% chrome steel. Foundry Trade J. 1960;108:562-563.

9 Schaeffler A. Constitution diagram for stainless steel weld metal. Metal Progress. 1949;56:680-680B.

10 Vilk J, Schneider A, Inden G. Martensitic/ferritic super heat-resistant 650°C steels: thermodynamics and kinetics of precipitation reactions. In: Proceedings of the 7th Liège Conference Materials for Advanced Power Engineering 2002 Part III. 2002; Liège, Belgium. Jülich, Germany: Forschungszentrum Jülich GmbH; 2002. p. 1299-1310.

11 Knezevic V, Balun J, Sauthoff G, Inden G, Schneider A. Design of martensitic/ferritic heat-resistant steels for application at 650°C with supporting thermodynamic modelling. Materials Science and Engineering. 2008;A477(1-2):334-343. http://dx.doi.org/10.1016/j.msea.2007.05.047.

12 Knezevic V, Sauthoff G, Vilk J, Inden G, Schneider A, Agamennone R, et al. Martensitic/ferritic super heat-resistant 650°C steels – design and testing of model alloys. ISIJ International. 2002;42(12):1505-1514. http://dx.doi.org/10.2355/isijinternational.42.1505.

13 Andersson JO, Ågren J. Models for numerical treatment of multicomponent diffusion in simple phases. Journal of Applied Physics. 1992;72(4):1350-1355. http://dx.doi.org/10.1063/1.351745.

14 Crusius S, Inden G, Knoop U, Höglund L, Ågren J. On the numerical treatment of moving boundary problems. Zeitschrift fur Metallkunde. 1992;83:673-678.

15 Crusius S, Höglund L, Knoop U, Inden G, Ågren J. On the growth of ferrite allotriomorphs in Fe-C. Z. Metallkde. 1992;83:729-738.

16 Inden G. Cinétique de transformation de phases dans des systems polyconstitués – aspects thermodynamiques. Entropie. 1997;202/203:6-14.

17 Borgenstam A, Höglund L, Ågren J, Engström A. DICTRA, a tool for simulation of diffusional transformations in alloys. J. Phase Equil. 2000;21(3):269-280. http://dx.doi.org/10.1361/105497100770340057.

18 Schneider A, Inden G. Simulation of the kinetics of precipitation reactions in ferritic steels. Acta Materialia. 2005;53(2):519-531. http://dx.doi.org/10.1016/j.actamat.2004.10.008.

19 Schneider A, Inden G. Computer simulation of diffusion controlled phase transformations. In: Raabe D, Roters F, Barlat F, Chen L-Q, editors. Continuum scale simulation of engineering materials. New York: Wiley-VCH; 2004.

20 Korcakova L, Hald J, Somers MAJ. Quantification of Laves phase particle size in 9CrW steel. Materials Characterization. 2001;47(2):111-117. http://dx.doi.org/10.1016/S1044-5803(01)00159-0.

21 Marinkovic BA, De Avillez RR, Kessler Barros S, Rizzo FC. Thermodynamic evaluation of carbide precipitates in 2.25Cr-1.0Mo steel for determination of service degradation. Materials Research. 2002;5:491-495. http://dx.doi.org/10.1590/S1516-14392002000400016.

22 Janovec J, Kroupa A, Svoboda M, Vyrostkova A, Grabke HJ. Evolution of secondary phases in Cr-V and Cr-Mo-V low alloy steels. Canadian Metallurgical Quarterly. 2005;44(2):219-232. http://dx.doi.org/10.1179/cmq.2005.44.2.219.

23 Danielsen HK, Hald J. A thermodynamic model oft he Z-phase Cr(V,Nb)N. Calphad. 2007;31(4):505-514. http://dx.doi.org/10.1016/j.calphad.2007.04.001.

24 Gustafson Å, Höglund L, Ågren J. Simulation of carbo-nitride coarsening in multicomponent Cr-steels for high temperature applications. In: Proceedings of the conference Advanced heat resistant steels for power generation. 1998; San Sebastian, Spain. London, England: IOM Communications; 1998.

25 Gustafson Å, Hättestrand M. Coarsening of precipitates in an advanced creep resistant 9% chromium steel: quantitative micrsocopy and simulations. Materials Science and Engineering A. 2002;333(1-2):279-286. http://dx.doi.org/10.1016/S0921-5093(01)01874-3.

26 Xiao X, Liu G, Hu B, Wang J, Ma W. Coarsening behavior for M23C6 carbide in 12%Cr-reduced activation ferrite/martensite steel: experimental study combined with DICTRA simulation. Journal of Materials Science. 2013;48(16):5410-5419. http://dx.doi.org/10.1007/s10853-013-7334-5.

27 Bjärbo A, Hättestrand M. Complex carbide growth, dissolution, and coarsening in a modified 12 pct chromium steel – an experimental and theoretical study. Metallurgical and Materials Transactions. A, Physical Metallurgy and Materials Science. 2001;32(1):19-27. http://dx.doi.org/10.1007/s11661-001-0247-y.

28 De Avillez RR, Marinkovic B, Da Costa e Silva ALV, Rizzo FC. Kinetics of carbide precipitation in a 2.25Cr-1Mo steel. Proc. of the 59th Annual ABM Congress – International, 2004.

29 Holzer I, Rajek J, Kozeschnik E, Cerjak H. Simulation of the precipitation kinetics during heat treatment and service of creep resistant martensitic 9-12% Cr steel. In: Proceedings of the 8th Liège Conference Materials for Advanced Power Engineering 2006 Part III. 2006; Liège, Belgium. Jülich, Germany: Forschungszentrum Jülich GmbH; 2006. p. 1191-1198.

30 Kozeschnik E, Pölt P, Brett S, Buchmayr B. Dissimilar 2.25Cr/9Cr and 2Cr/0.5CrMoV steel welds: part 1: characterisation of weld zone and numerical simulation. Science Techn. Weld. Join. 2002;7(2):63-68. http://dx.doi.org/10.1179/136217102225003005.

31 Sonderegger B, Hacksteiner M, Mendez-Martin F, Holzer I, Kozeschnik E. Calculation of phase boundary energies and application in multicomponent steels. In: Proceedings of the 9th Liège Conference Materials for Advanced Power Engineering 2010 Part III. 2010; Liège, Belgium. Jülich, Germany: Forschungszentrum Jülich GmbH; 2010. p. 320-329.

Received: 5 Feb. 2016
Accepted: 5 Feb. 2016